Open Access

Iraqi Journal of Industrial Research (IJOIR)

Journal homepage: http://ijoir.gov.iq

Theoretical Evaluation of Natural Tantalum Oxides for Gamma-Ray Shielding via Phy-X software

Taher Toman Taher*

Iraqi Atomic Energy Commission, Iraq

Article information

Article history:
Received: August, 18, 2025
Accepted: November, 01, 2025
Available online: December, 14, 2025

Keywords:
Gamma rays shielding,
Tantalum compounds,
Phy-X software

Corresponding Author:
Taher Toman Taher
tahert4477@gmail.com

DOI:
https://doi.org/10.53523/ijoirVol12I2ID597

Abstract

This study utilized multiple materials to protect workers, particularly those in oil fields, from radiation hazards, including gamma rays. Each sample from the eight tantalum oxides: $Mn^{2+}Sn^{4+}Ta_2O_8$, $Mn^{2+}Ta_2O_6$, $Fe^{2+}Ta_2O_6$, $Fe^{2+}Ta_2O_6$, $(Y,U,Fe^{2+})(Ta,Nb)(O.OH)_4$, $Bi(Ta,Nb)O_4$, $(Ca,Na)_2(Ta,Nb)_2O_6F$, and $Al_4Ta_3O_{13}(OH)$ were evaluated as shields from the harm of gamma rays. All these materials are natural and insoluble in water. Here, the potential of using tantalum oxides mainly depends on the chemical composition of each material and its density, as well as their effectiveness in mitigating ionizing radiation. The calculated gamma ray shielding parameters include the linear attenuation coefficient, mass attenuation coefficient, half value layer, tenth value layer, mean free path, effective electron density, effective conductivity, and atomic cross-section. Electronic cross section, effective atomic number, and equivalent atomic number. These parameters were obtained by applying free Phy-X software within the photon interaction range of 0.015-15 MeV. The linear attenuation coefficient and mass attenuation coefficient decreased as the energy increased, whereas the other shielding parameters decreased as the energy decreased. Among all the tested samples, bismutotantalite $Bi(Ta,Nb)O_4$ proved as the most effective material for gamma-ray shielding because of its heavy element content, high mean atomic number, and highest density, which are the key factors at intermediate energies (Compton effect). In contrast, materials such as {$(Ca,Na)_2(Ta,Nb)_2O_6F$, $Al_4Ta_3O_{13}(OH)$, $(Y,U,Fe^{2+})(Ta,Nb)(O.\ OH)_4$}, which contain lighter elements were less effective in protection from this radiation. At high photon energies, pair production occurs; consequently, these lighter materials do not strongly absorb radiation.

1. Introduction

Natural and artificial radiations have serious impacts on humans and the environment. Gamma rays are ionizing radiation that may cause mutation or injury to biological tissues and prompt cancer or genetic diseases. These important topics have been explored via experimental and theoretical methodologies with various materials. These studies ensured that protection mainly depended on the exposure dose, distance, time, and chemical composition of the tested material. Each material is defined as a radioactive material according to the emitted

radiation or particles per unit time (second). To overcome radiation risk via experimental methodology, physical and chemical characterization, time, and cost are the main parameters for choosing any shield substance that provides a healthy, safe working environment with optimum management regulations in industry, gas and petroleum production sites, health centers, academic laboratories, and others [1-4].

To overcome the experimental toxicity, time, cost consuming and their related errors, many researchers have presented theoretical gamma attention parameters according to their chemical–physical properties, such as density and chemical formula. It will be easier for any researcher in academic or industrial sectors to understand material behaviour towards radiation diffusion and penetration through the following attention parameters: the mass attenuation coefficient, effective atomic number, and other parameters. Numerous computerized simulations, such as XCOM, Phy-X/PSD, NGCAL, and others, have been performed to calculate the attenuation or photoelectric absorption depending on the density (ρ) and Effective Atomic Number. These computer-based models have several limitations [5-24]. Phy-X/PSD is a downloadable (or online) model with an energy range (0.015–15) MeV requiring an academic email for registration to predict the efficiency of identified elements, compounds, and other materials that naturally occur or were synthesized in the laboratory [9, 25].

Natural materials are excellent choices for radiation attenuation, especially in the oil and petroleum sectors, which address naturally occurring radioactive materials (NORMs) containing Potassium (K), Thorium (Th), or Uranium (U) and releasing Radium (Ra) and Radon (Rn). By depending on natural shielders, the cost of preparation can be reduced. Here, a theoretical study aims to evaluate various gamma ray attenuation coefficients of tantalum oxides within a specific energy range (0.015-15) MeV by using the online Phy-X software. In this study, the calculated gamma ray shielding parameters include the Linear Attenuation Coefficient (LAC), Mass Attenuation Coefficient (MAC), Half Value Layer (HVL), Tenth Value Layer (TVL), Mean Free Path (MFP), Effective Electron Density (Neff), Effective Atomic Number (Zeff), and Equivalent Atomic Number (Zeq). These calculated coefficients describe the properties of radiation absorption and its interaction with materials. Additionally, they help researchers and others who are involved in radiation protection to understand and identify the best material for radiation shielding, depending on natural-based tantalum materials, which are useful in many applications, such as medical and industrial sectors, and nuclear reactors.

2. Experimental Procedure

2.1. Chemicals

The tested materials were eight oxides: Wodginite ($Mn^{2+}Sn^{4+}Ta_2O_8$), Tantalite-(Mn)($Mn^{2+}Ta_2O_6$), Tantalite-(Fe) ($Fe^{2+}Ta_2O_6$), Tapiolite-(Fe) ($Fe^{2+}Ta_2O_6$), Yttrotantalite-(Y)((Y,U,Fe^{2+})(Ta,Nb)$(O,OH)_4$), Bismutotantalite ($Bi(Ta,Nb)O_4$), Fluorcalciomicrolite ($(Ca,Na)_2(Ta,Nb)_2O_6F$), and Simpsonite ($Al_4Ta_3O_{13}(OH)$), which were coded T1,T2,T3,T4,T5,T6,T7, and T8, as shown in Table (1) and Figure (1).

Table (1) shows the most characteristic information related to the tested materials, as mentioned in reference [26], whereas the percentage composition (%) was computed via Phy-X software. Additionally, the mean atomic number, $\bar{Z}$, was computed according to references [17, 20, 25]. Figure (1) shows the natural crystal form of each material according to reference [26].

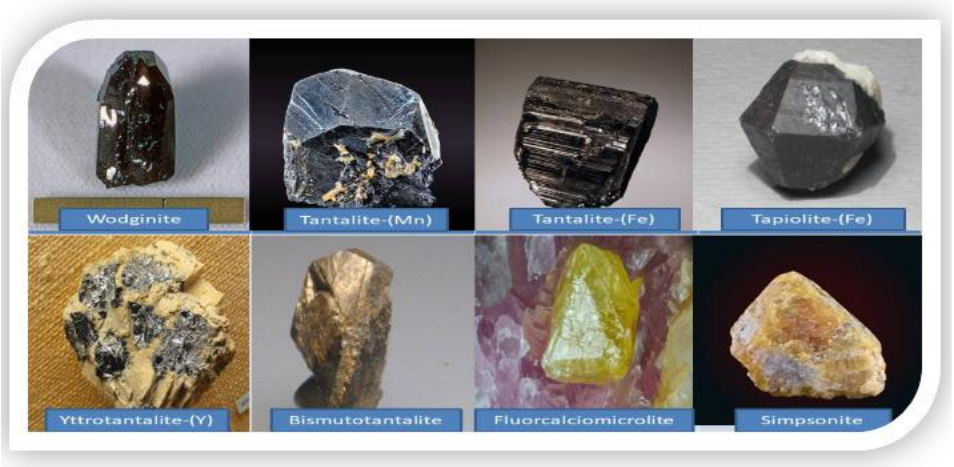

Figure (1): Images of the tested materials [26].

Table (1): Several characteristics of the tested oxide complexes [17, 20, 25, 26].

Code	Name, chemical formula	General specifications	Density, gm/cm^3	Percentage Composition, %		Mean Atomic Number, $\bar{Z}$
T1	**Wodginite** $Mn^{2+}Sn^{4+}Ta_2O_8$	Colour: Red–brown, dark brown to black Hardness:5½ Crystal System:Monoclinic Morphology:Crystals commonly flattened, dipyramidal or prismatic	7.19	Mn	0.1022	28.75
				Sn	0.4419	
				Ta	0.3368	
				O	0.1191	
T2	**Tantalite-(Mn)** $Mn^{2+}Ta_2O_6$	Colour: Pink to nearly colourless, reddish brown to black Hardness: 6 Crystal System: Orthorhombic Morphology: Short prismatic to tabular	6.65	Mn	0.1935	24.4
				Ta	0.6374	
				O	0.1691	
T3	**Tantalite-(Fe)** $Fe^{2+}Ta_2O_6$	Colour: Iron-black Hardness: 6 - 6½ Crystal System: Orthorhombic Morphology: Exsolution intergrowths with ferrotapiolite.	6.65	Fe	0.1961	24.6
				Ta	0.6354	
				O	0.1685	
T4	**Tapiolite-(Fe)** $Fe^{2+}Ta_2O_6$	Colour: Black Hardness:6 - 6½ Crystal System: Tetragonal Morphology: Short prismatic, nearly equant, rarely elongated.	7.9	Fe	0.1961	24.6
				Ta	0.6354	
				O	0.1685	
T5	**Yttrotantalite-(Y)** $(Y,U,Fe^{2+})(Ta,Nb)(O,OH)_4$	Colour: Brown–black to black Hardness: 5 - 5½ Crystal System: Orthorhombic Morphology: Prismatic [001] with {110} and {010} prominent; also tabular {010}.	5.5	Y	0.1289	19.21
				U	0.3451	
				Fe	0.0810	
				Ta	0.2624	
				Nb	0.1347	
				O	0.0464	
				H	0.0015	
T6	**Bismutotantalite** $Bi(Ta,Nb)O_4$	Colour: Light brown to pitch-black Hardness: 5 - 5½ Crystal System: Orthorhombic Morphology: Stout crystals, prismatic on [001]	8.15	Bi	0.4189	32.71
				Ta	0.3627	
				Nb	0.1862	
				O	0.0321	
T7	**Fluorcalciomicrolite**	Colour: Colourless	6.16	Ca	0.1078	23.13

Code	Name, chemical formula	General specifications	Density, gm/cm^3	Percentage Composition, %		Mean Atomic Number, $\bar{Z}$
	$(Ca,Na)_2(Ta,Nb)_2O_6F$	Hardness: 4 – 5 Crystal System: Isometric		Na	0.0618	
				Ta	0.4865	
				Nb	0.2498	
				O	0.0430	
				F	0.0511	
T8	**Simpsonite $Al_4Ta_3O_{13}(OH)$**	Colour: Yellow, light brown or colourless, gray Hardness: 7 - 7½ Crystal System: Trigonal Morphology: Crystals tabular to short prismatic.	6.35	Al	0.1232	17.45
				Ta	0.6198	
				O	0.2558	
				H	0.0012	

3. Theoretical Part

All the theoretical parameters can be calculated via Phy-X software [9], including the linear attenuation coefficient (LAC), mass attenuation coefficient (MAC), half value layer (HVL), tenth value layer (TVL), mean free path (MFP), effective electron density (Neff), effective atomic number (Zeff), and equivalent atomic number (Zeq), which were calculated and discussed for each sample (T1 to T8). Figures (2-5) show the variation in each shielding parameter at all energies for all the materials. Tables (2 & 3) present the resulting LAC and MAC of each material according to the tested energy (0.015-15) MeV.

Table (2): LAC results of each material according to their energy values.

Energy, MeV	T1	T2	T3	T4	T5	T6	T7	T8
1.50E-02	511.231	634.842	642.769	763.590	379.157	833.178	465.609	536.724
2.00E-02	238.855	298.451	302.095	358.880	343.704	610.134	318.501	253.419
3.00E-02	189.476	102.330	103.504	122.960	149.947	212.825	109.790	87.593
4.00E-02	89.098	47.837	48.351	57.440	70.741	100.009	51.085	41.231
5.00E-02	49.279	26.683	26.951	32.017	39.472	55.651	28.270	23.143
6.00E-02	30.442	16.705	16.864	20.034	24.555	34.588	17.534	14.576
8.00E-02	28.528	33.032	33.022	39.229	20.218	33.896	25.997	30.297
1.00E-01	16.120	18.836	18.829	22.368	11.533	33.917	14.803	17.314
1.50E-01	5.894	6.878	6.877	8.169	7.805	12.282	5.446	6.356
2.00E-01	3.084	3.539	3.540	4.205	3.985	6.163	2.845	3.289
3.00E-01	1.453	1.592	1.594	1.893	1.710	2.587	1.326	1.496
4.00E-01	0.972	1.022	1.024	1.217	1.042	1.555	0.877	0.970
5.00E-01	0.760	0.777	0.779	0.925	0.758	1.122	0.681	0.741
6.00E-01	0.643	0.644	0.646	0.767	0.607	0.894	0.572	0.617
8.00E-01	0.514	0.502	0.504	0.599	0.453	0.664	0.454	0.484
1.00E+00	0.441	0.425	0.427	0.507	0.373	0.546	0.389	0.411
1.50E+00	0.347	0.331	0.332	0.395	0.282	0.413	0.305	0.320
2.00E+00	0.306	0.291	0.292	0.347	0.248	0.365	0.268	0.281
3.00E+00	0.272	0.258	0.259	0.308	0.222	0.331	0.237	0.246
4.00E+00	0.261	0.247	0.248	0.294	0.215	0.325	0.226	0.233
5.00E+00	0.258	0.243	0.245	0.291	0.214	0.328	0.222	0.228
6.00E+00	0.259	0.244	0.245	0.292	0.217	0.334	0.223	0.227
8.00E+00	0.266	0.251	0.252	0.300	0.226	0.352	0.228	0.231
1.00E+01	0.277	0.260	0.262	0.311	0.237	0.372	0.236	0.238
1.50E+01	0.304	0.286	0.287	0.341	0.265	0.418	0.258	0.258

Table (3): MAC results of each material according to their energy values.

Energy, MeV	T1	T2	T3	T4	T5	T6	T7	T8
1.50E-02	71.103	95.465	96.657	96.657	68.938	102.230	75.586	84.524
2.00E-02	33.220	44.880	45.428	45.428	62.492	74.863	51.705	39.908
3.00E-02	26.353	15.388	15.565	15.565	27.263	26.114	17.823	13.794
4.00E-02	12.392	7.194	7.271	7.271	12.862	12.271	8.293	6.493
5.00E-02	6.854	4.012	4.053	4.053	7.177	6.828	4.589	3.645
6.00E-02	4.234	2.512	2.536	2.536	4.465	4.244	2.846	2.295
8.00E-02	3.968	4.967	4.966	4.966	3.676	4.159	4.220	4.771
1.00E-01	2.242	2.833	2.831	2.831	2.097	4.162	2.403	2.727
1.50E-01	0.820	1.034	1.034	1.034	1.419	1.507	0.884	1.001
2.00E-01	0.429	0.532	0.532	0.532	0.725	0.756	0.462	0.518
3.00E-01	0.202	0.239	0.240	0.240	0.311	0.317	0.215	0.236
4.00E-01	0.135	0.154	0.154	0.154	0.190	0.191	0.142	0.153
5.00E-01	0.106	0.117	0.117	0.117	0.138	0.138	0.111	0.117
6.00E-01	0.089	0.097	0.097	0.097	0.110	0.110	0.093	0.097
8.00E-01	0.071	0.076	0.076	0.076	0.082	0.081	0.074	0.076
1.00E+00	0.061	0.064	0.064	0.064	0.068	0.067	0.063	0.065
1.50E+00	0.048	0.050	0.050	0.050	0.051	0.051	0.049	0.050
2.00E+00	0.043	0.044	0.044	0.044	0.045	0.045	0.044	0.044
3.00E+00	0.038	0.039	0.039	0.039	0.040	0.041	0.038	0.039
4.00E+00	0.036	0.037	0.037	0.037	0.039	0.040	0.037	0.037
5.00E+00	0.036	0.037	0.037	0.037	0.039	0.040	0.036	0.036
6.00E+00	0.036	0.037	0.037	0.037	0.039	0.040	0.036	0.036
8.00E+00	0.037	0.038	0.038	0.038	0.041	0.043	0.037	0.037
1.00E+01	0.039	0.039	0.039	0.039	0.043	0.046	0.038	0.037
1.50E+01	0.042	0.043	0.043	0.043	0.048	0.051	0.042	0.041

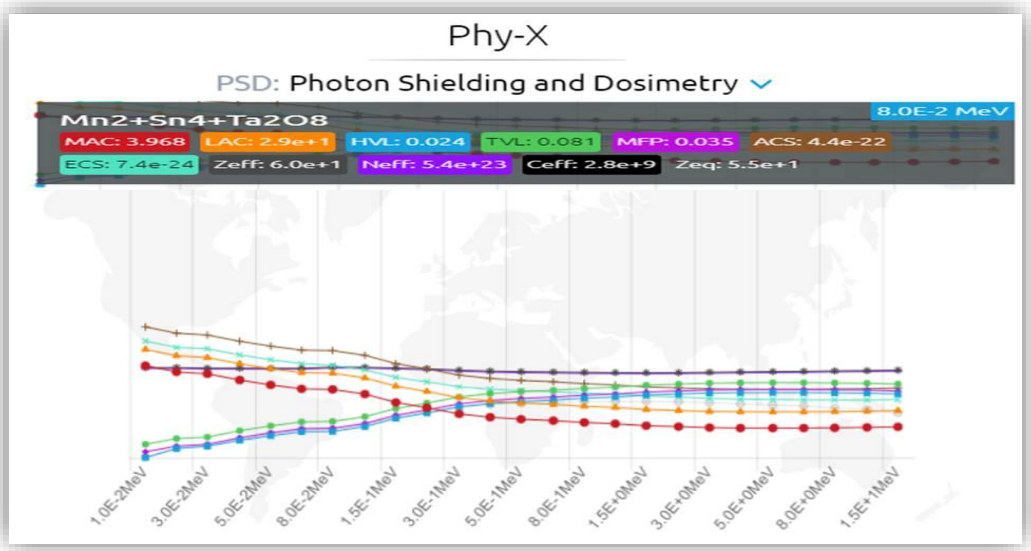

Figure (2a): Gamma radiation behaviour of T1.

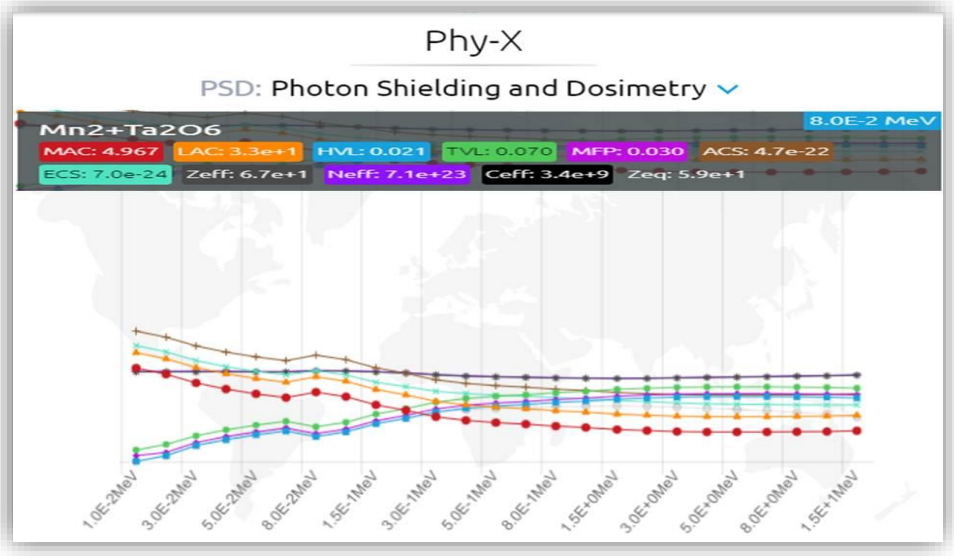

Figure (2b): Gamma radiation behaviour of T2.

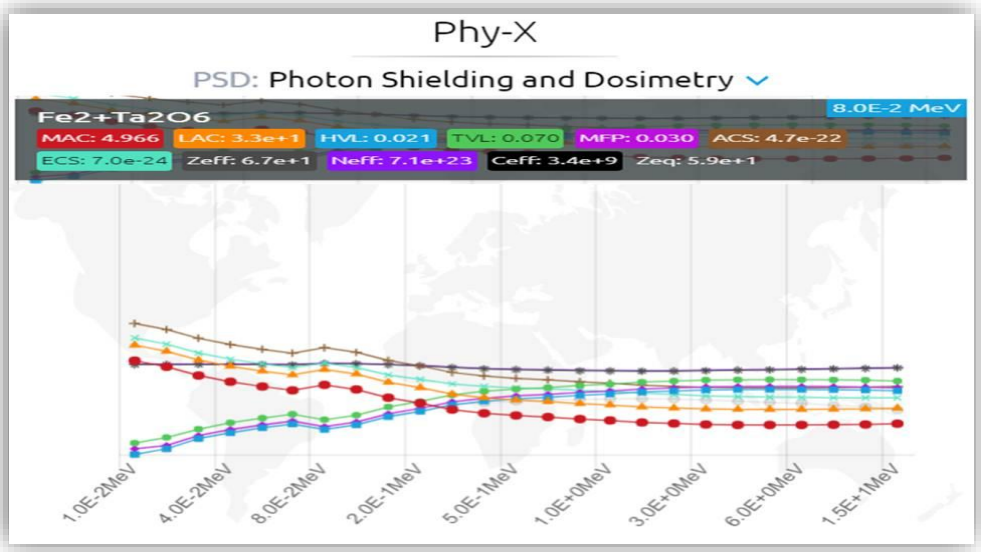

Figure (3a): Gamma radiation behaviour of T3.

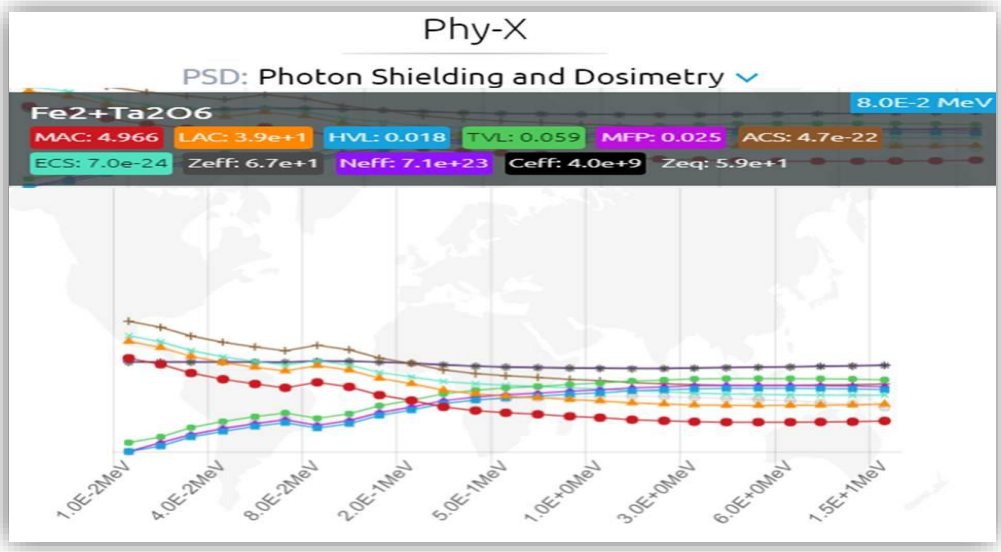

Figure (3b): Gamma radiation behaviour of T4.

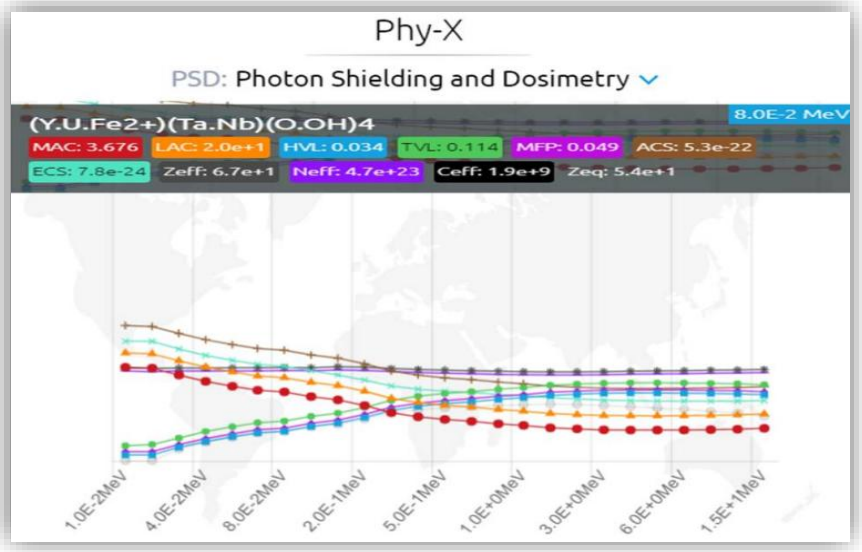

Figure (4a): Gamma radiation behaviour of T5.

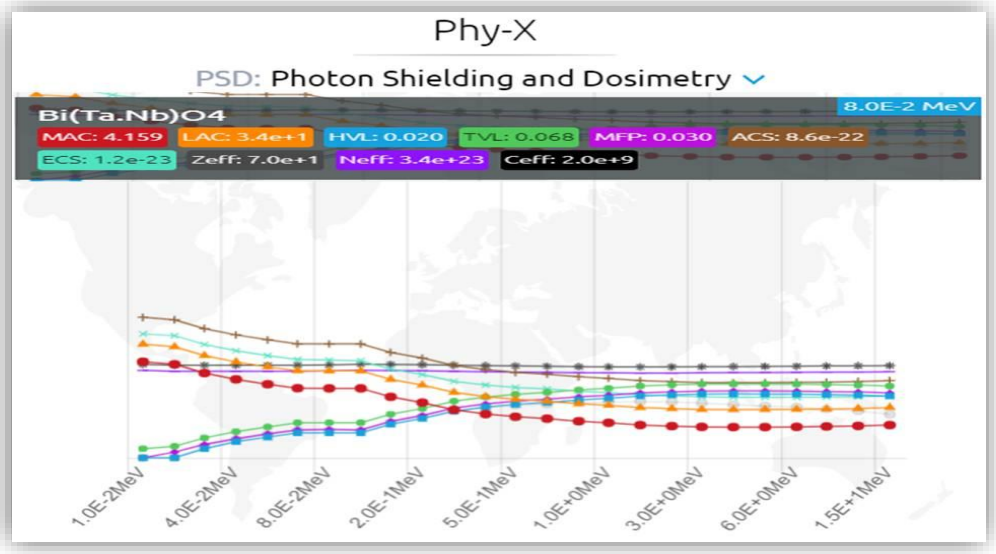

Figure (4b): Gamma radiation behaviour of T6.

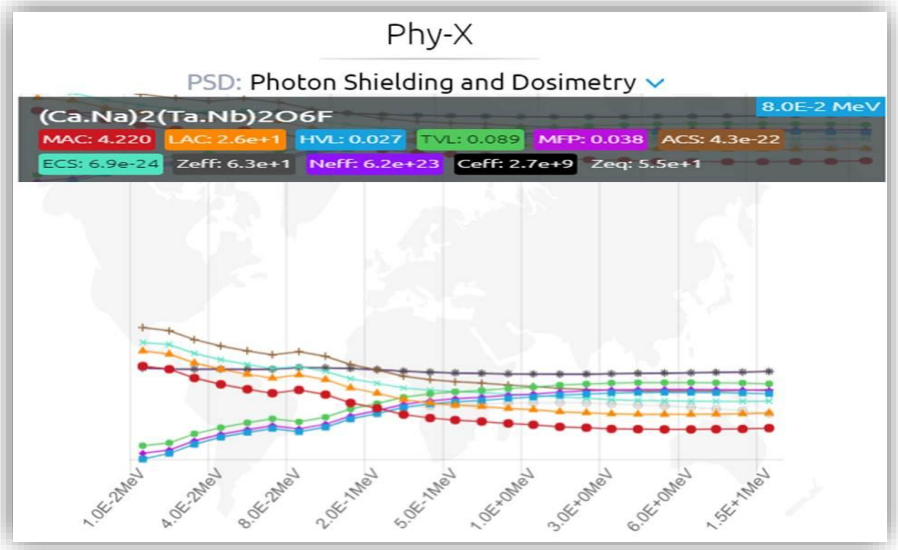

Figure (5a): Gamma radiation behaviour of T7.

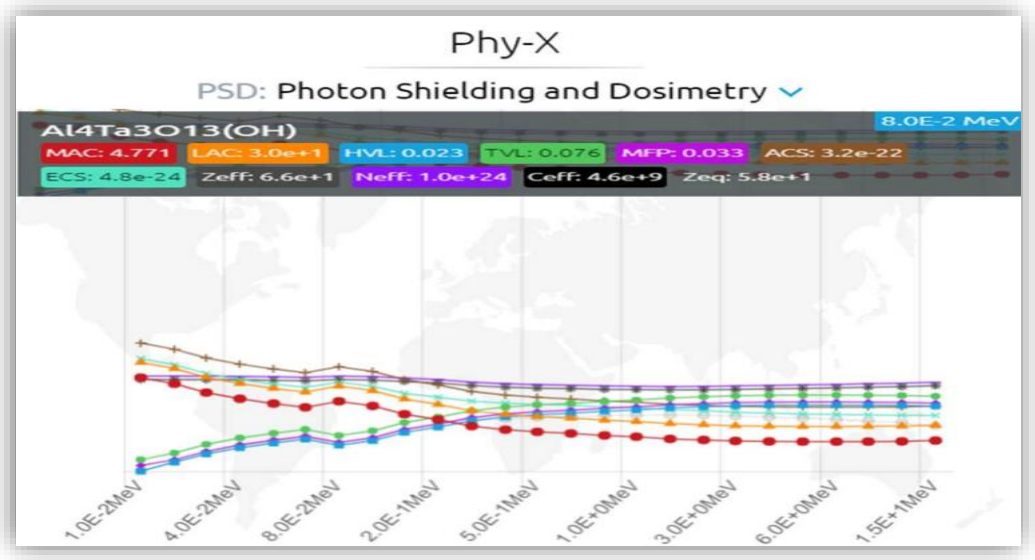

Figure (5b): Gamma radiation behaviour of T8.

4. Results and Discussion

In general, a gamma ray is a penetrating form of electromagnetic radiation arising from the radioactive decay of atomic nuclei. It consists of the shortest wavelength electromagnetic waves, typically shorter than those of X-rays. Many factors that affect our attention calculations include density, composition differences, the atomic weights of elements, and the number of oxygen atoms. The harmful impact of radiation on humans and the environment, especially tissues and organs, is well known and may arise from direct or indirect interactions with radioactive sources, including naturally occurring radioactive materials (NORMs). Many studies have estimated the gamma radiation shielding parameters of alloys, composites, polymers, polymer concretes, and ceramics [11-29].

Experimental studies are highly common in nuclear science and technology. Although computer-based models have been applied to minimize time, cost, errors, toxicity, etc.

Now, it is currently preferable to evaluate attenuation characteristics, including XCOM, NGCAL, Phy-X/PSD and others. Both simulation calculations and practical studies have shown that the excellent radiation attenuator has a high density and Effective Atomic Number [1-24].

This study aims to protect researchers and workers in the radiation sectors, particularly in oil fields, from the risks of gamma rays. In this new Iraqi study, eight natural tantalum oxides were evaluated for the first time as gamma shielders via an eco-friendly computerized model known as Phy-X. These tantalum oxides in this theoretical study are insoluble in water and have various chemical formulas: {$Mn^{2+}Sn^{4+}Ta_2O_8$, $Mn^{2+}Ta_2O_6$, $Fe^{2+}Ta_2O_6$, $Fe^{2+}Ta_2O_6$, $(Y,U,Fe^{2+})(Ta,Nb)(O.\ OH)_4$, $Bi(Ta,Nb)O_4$, $(Ca,Na)_2(Ta,Nb)_2O_6F$, $Al_4Ta_3O_{13}(OH)$}. The calculated gamma ray shielding parameters are Linear Attenuation Coefficient (LAC), Mass Attenuation Coefficient (MAC), Half Value Layer (HVL), Tenth value layer (TVL), Mean free path (MFP), Effective Electron Density (N_{eff}), Effective Conductivity (C_{eff}), and Atomic cross section (ACS). Electronic cross section (ECS), Effective Atomic Number (Z_{eff}), Equivalent Atomic number (Z_{eq}).

4.1. Linear Attenuation Coefficient

LAC (**cm^{-1}**) describes the fraction of the absorbed or scattered gamma rays per unit thickness of the tested material. In fact, LAC value provides a numerical identification of atoms per cm^3 of the target material, in addition to the probability of a photon under scattering or absorption interactions. This coefficient represents a master key parameter in attenuation calculations that reflects the interaction between gamma radiation and incident matter. It mainly depends on the Lambert–Beer equation (1):

$$\mu = ((\ln(I/I_0))/x) \ldots\ldots\ldots (1)$$

Where: **μ**: Linear Attenuation Coefficient, **I_0:** intensity of the incident photon, **I:** transmitted photons through the absorbed material having, and **x**: thickness (cm).

In this study, LAC depends on the chemical composition, density, radiation energy, and atomic number of matter, where the mean atomic number of the tested material has a proportional relationship with the attenuation process. In general, the LAC parameter decreases with increasing applied energy [25].

In addition, the composition percentages of Ta and O varied in their effects on the shielding efficiency, where the Ta% sequence presented the highest value of T4, whereas the highest O% was T2. Both the Ta% and O% relationships with LAC were influenced by the composition percentage of the other elements in each tested material, which, in the final summary, represents the density and mean atomic number impacts (Table 2, Figures (2-6)).

Ta%: T5, T1, T6, T7, T8, T3. T4, T2

O%: T6, T7, T5, T1, T3. T4, T2, T8

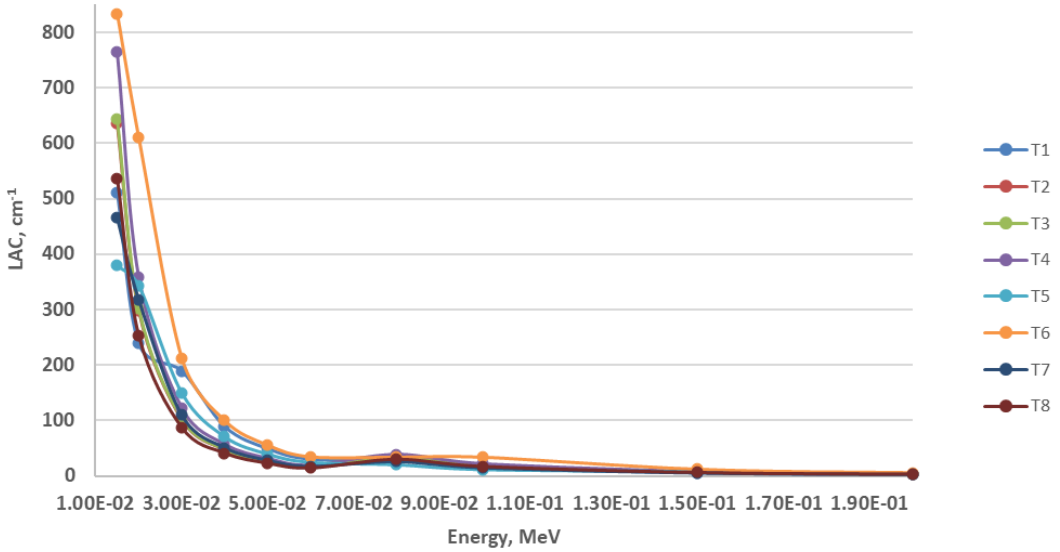

Figure (6): Gamma shielding by the tested material according to the LAC results.

From Table (2) and Figures (2-6), the LAC sequence from the lowest to the highest ([T7. T8], T5, T2, T3, T1, T4, and T6) showed that T6 ($Bi(Ta,Nb)O_4$) was a superior gamma shielding material among all the tested materials. In general, the LAC sequence is considered semiidentical to the sequence of densities (T5, T7, T8, [T2. T3], T1, T4, T6) (Tables 1 and 2).

4.2. The Mass Attenuation Coefficient (MAC)

To identify how radiation acts with a material, the MAC ($cm^2\ g^{-1}$) explains this phenomenon, where it depends on density (ρ) and LAC data.

$$MAC = \mu/\rho \ldots\ldots\ldots (2)$$

Where: **μ**: Linear Attenuation Coefficient, and **ρ:** density. Here, the MAC decreased with increasing energy [0.015→ 5] MeV and then increased from an energy of 8 MeV. Since $Bi(Ta,Nb)O_4$ has the highest density, it is more resistant to radiation penetration and absorbs a greater amount of energy (Figure 7, Table 3).

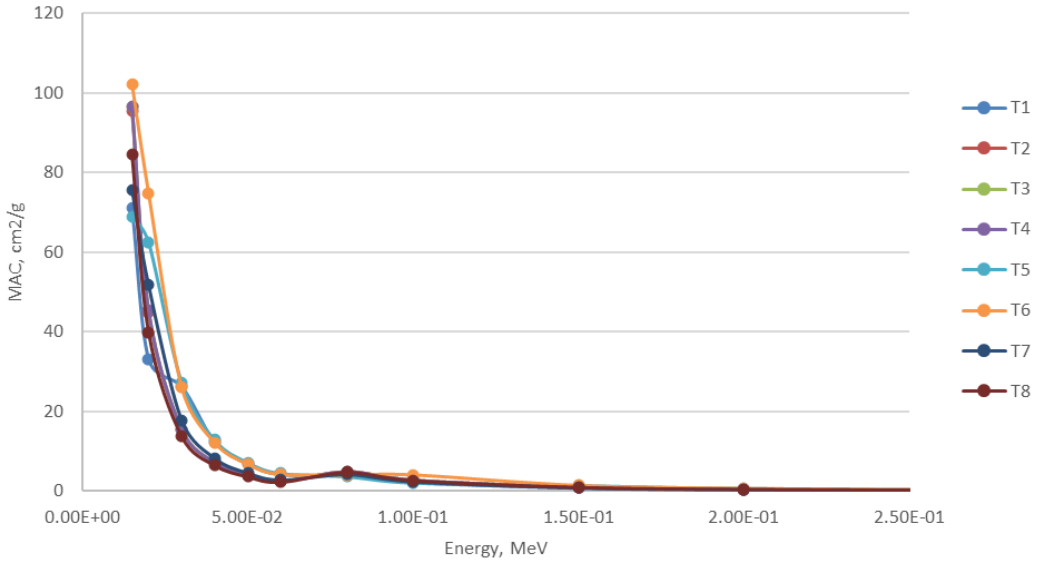

Figure (7): Gamma shielding by the tested material according to the MAC results.

It can be concluded from both the LAC and MAC results (Tables 2 & 3, Figures 2-7) that:

- At low energies, the photoelectric effect governs, where both the linear and mass attenuation coefficients are inversely proportional to energy, whereas as the energy increases, both coefficients decrease sharply.
- At medium energies, the Compton effect is controlled, the LAC and MAC slowly decrease, and
- At high energies, pair formation begins, and the linear and mass absorption coefficients increase with energy.

4.3. Half Value Layer (HVL)

$$HVL = \ln 2/\mu \quad \ldots\ldots\ldots (3)$$

Where: **μ**: Linear Attenuation Coefficient. The half value layer (HVL, cm) is an important parameter for radiation shielding because it identifies the thickness of a material that has the ability to absorb ≥ 50% of the received radiation. The HVL increased with increasing energy and then decreased above an energy of 6 MeV (Figure 8). It depends on the material type and the energy of the photon. The higher the linear attenuation coefficient is, the smaller the half Value Layer is.

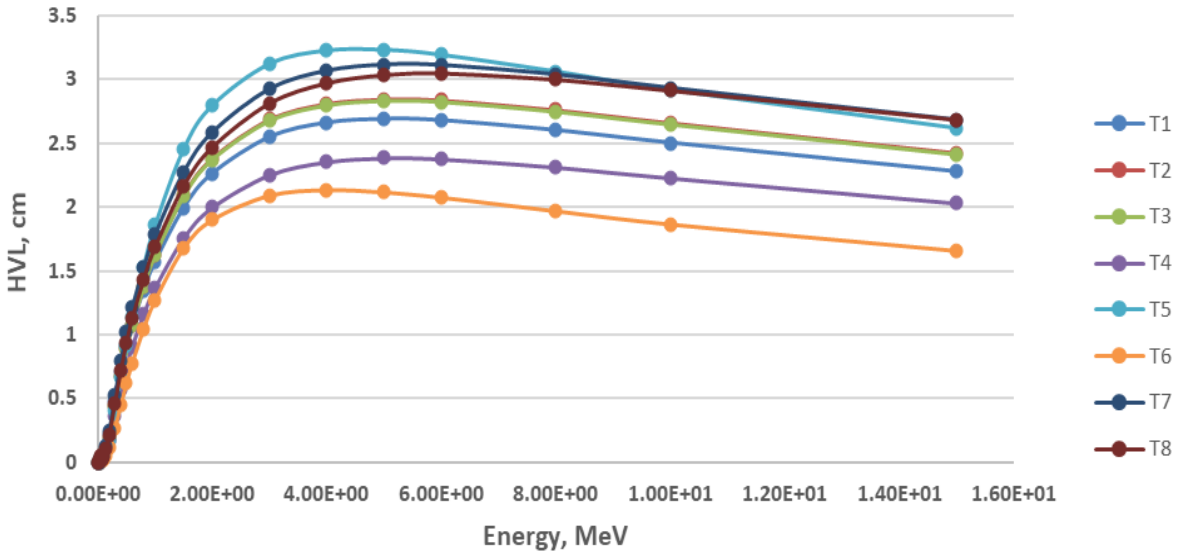

Figure (8): Gamma shielding by the tested material according to the HVL results.

4.4. Tenth Value Layer (TVL)

This characteristic describes the thickness that reduces incident radiation to a value of one-tenth

$$TVL = \ln 10/\mu \ldots\ldots\ldots (4)$$

Where: **μ-** Linear Attenuation Coefficient. In general, TVL (cm) increased with increasing energy, except that energy ≥ 6 MeV decreased. This may be related to radiation attenuation with the material, especially the absorption of 90% of the incident radiation at this depth (or thickness) (Figure 9). It depends on the type of ray and on the properties of the material, including its density and atomic number.

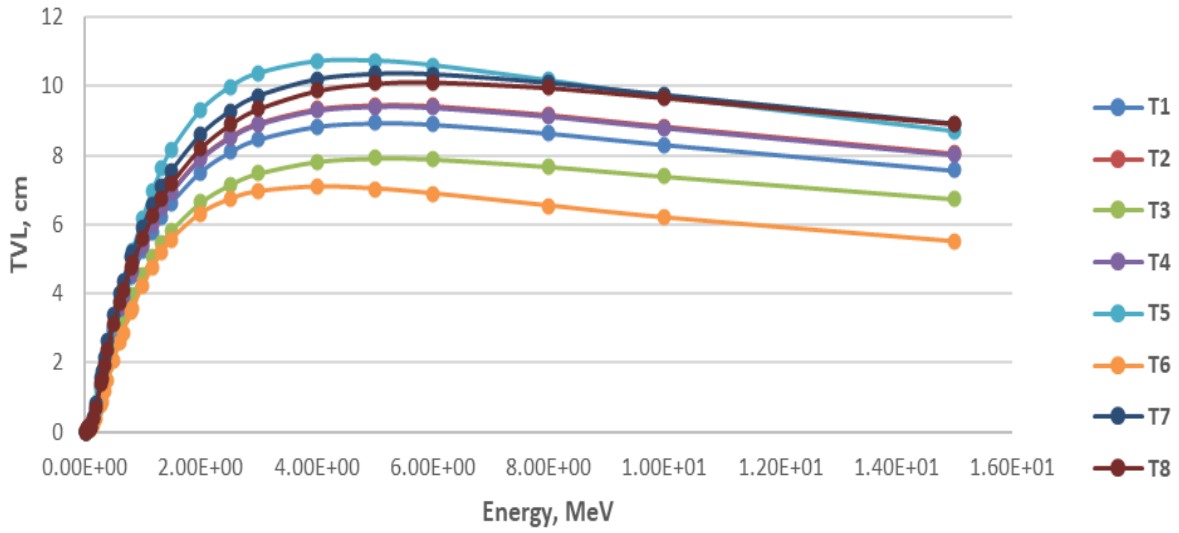

Figure (9): Gamma shielding by the tested material according to the TVL results.

4.5. Mean Free Path (MFP)

This is another calculated property that indicates the distance travelled by the incident radiation—here, gamma rays—before its direction is changed by successive collisions with matter. This collision changes the initial momentum of the incident photon with matter through scattering or absorption interactions. As the energy of a

particle increases, its speed increases, making it less likely to interact with atoms or electrons in the material. Thus, the mean free path increases with increasing energy, up to a certain point (Figure 10).

In some cases (such as nuclear or photon reactions), increasing energy may increase the probability of a reaction, and thus reduce the MFP.

$$\mathbf{MFP = 1/\mu \ldots\ldots\ldots (5)}$$

Where: **μ**- Linear Attenuation Coefficient. MFP (cm) mainly depends on the density of the medium through which it travels.

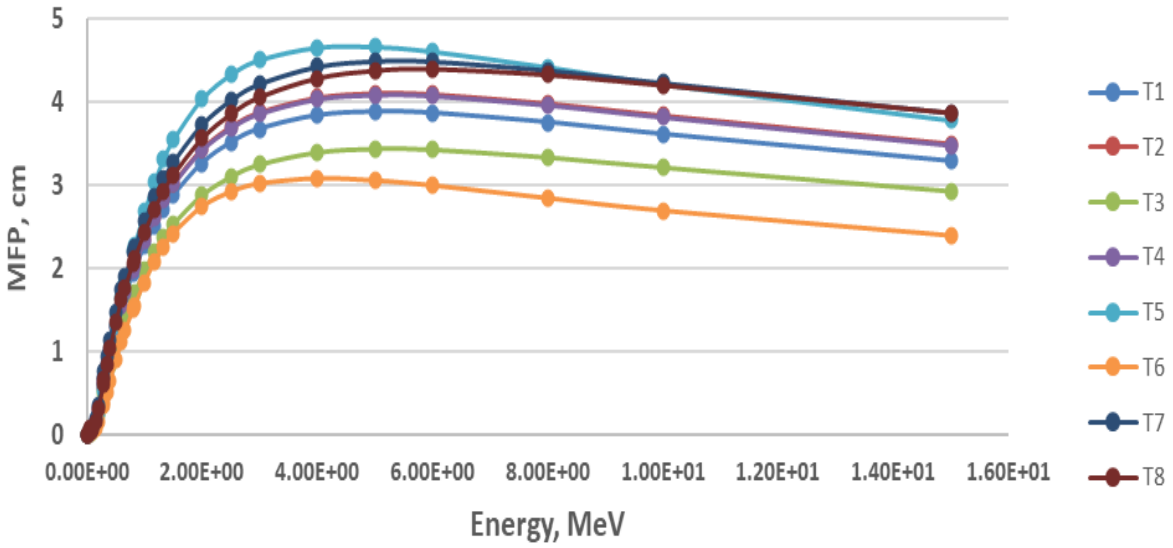

Figure (10): Gamma shielding by the tested material according to the MFP results.

4.6. Effective Electron Density (N_{eff})

The number of electrons per unit volume (**electron/cm^3**) that can participate in the physical reactions of a given substance. Equation (1) shows the influence of the material composition and density on the resulting effective electron density. In addition, the higher the energy is, the more electrons contribute to physical reactions (Figure 11). A sufficient amount of absorbed energy (high-energy photons) releases electrons via the photoelectric effect.

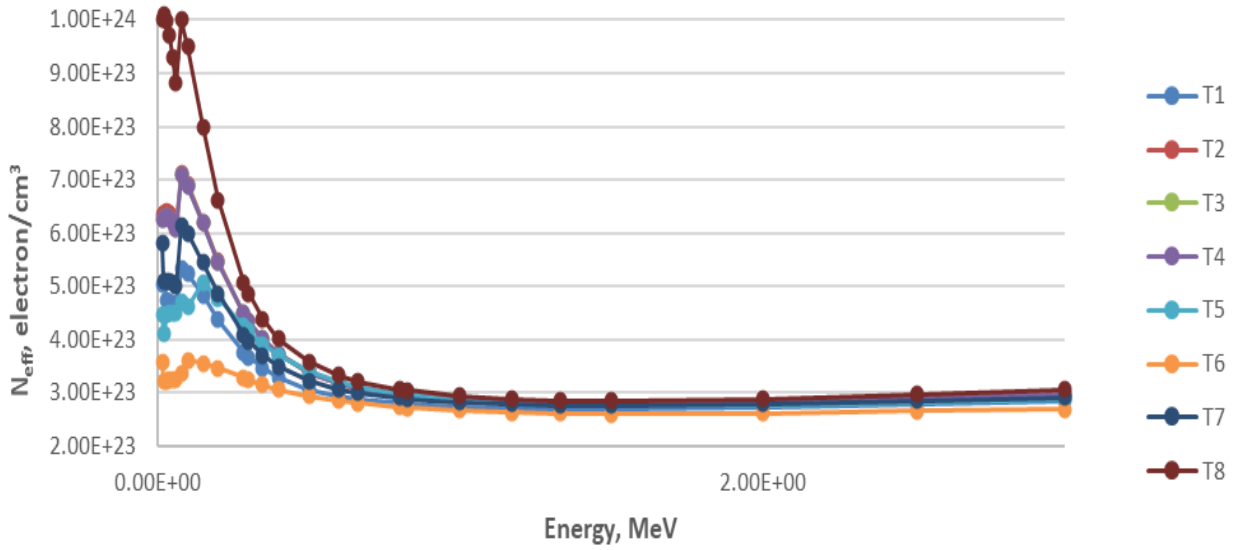

Figure (11): Gamma shielding by the tested material according to the N_{eff} results.

These reactions depend on the number of electrons available in the atoms, not just on mass or density. The electron density is closely associated with the effective atomic number, which is based on the interaction mechanism.

$$N_{eff} = (N_A \cdot Z_{eff} \cdot \rho)/A \text{ …… (6)}$$

Where: N_A**:** Avogadro's Number mol^{-1}, Z_{eff} **:** Effective atomic number, **ρ:** Mass density of matter g/cm^3, and **A**: Atomic or molecular mass g/mol.

4.7. Effective Conductivity (C_{eff})

This property determines how radiation (photon or electron) interacts with the material in terms of the propagation of radiation within the medium (Equation 2). It is highly related to other tested parameters, N_{eff} (or the number of electrons), and the MFP. Conductivity refers to the flow of electrons under radiation influence (N_{eff}) and the distance travelled by gamma rays with successive collisions in terms of scattering or absorption interactions (MFPs). Figure (12) shows the effects of increasing energy and other parameters on decreasing conductivity.

$$C_{eff} = (Neff \times \rho \times e^2 \times \tau \times m_e)/10^3 \text{ …… (7)}$$

Where: N_{eff}: effective number of electrons per unit volume of the material, **ρ**: density of the material, **e:** elementary charge, **τ**: mean free path of an electron in the material, and m_e: the mass of an electron.

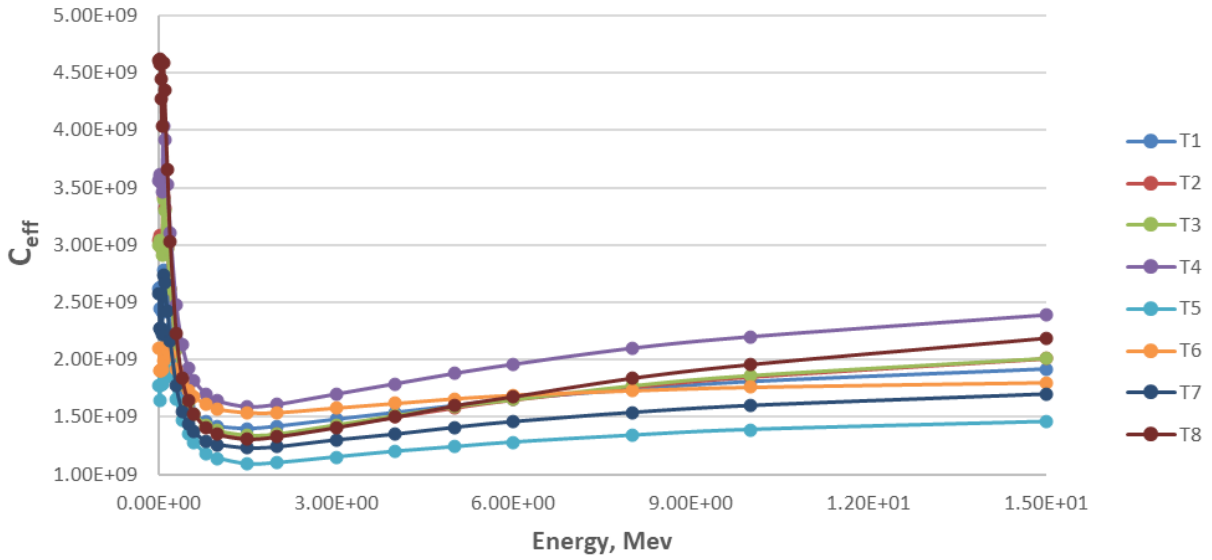

Figure (12): Gamma shielding by the tested material according to the C_{eff} results.

4.8. Atomic Cross Section (ACS)

By calculating the Atomic Cross Section **(ACS),** the probability of the ionization or scattering interaction between a photon or electron and the nucleus of an atom depends on the type of reactant, the interaction, and the nature of the target. These essential factors determine the decrease in the ACS with increasing energy (Figure 13).

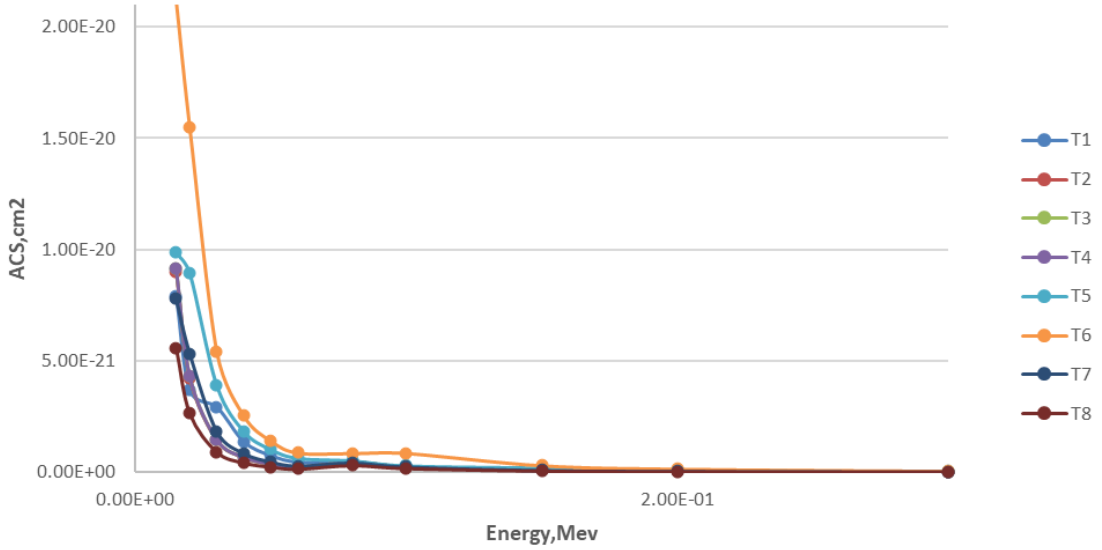

Figure (13): Gamma shielding by the tested material according to the ACS results.

4.9. Electronic Cross Section (ECS)

The electronic cross section (ECS) refers to the effective area where gamma rays interact with atomic electrons in the target. Increasing these interactions reflects a high probability of interaction of the incident photon, where a high thickness and high energy minimize the number of observed events towards low ECS results. Figure (14) shows the effects of changes in energy on the ECS results, which vary with other physical material properties.

$$\Sigma = N_{interactions}/N_{incident} \cdot n \cdot x \ \ldots\ldots\ldots (8)$$

Where: **σ**: cross section (m^2), $\mathbf{N}_{interactions}$: number of observed interaction events, $\mathbf{N}_{incident}$: number of incident particles, **n**: density of target particles (per m^3), and **x**: thickness of the target (m)

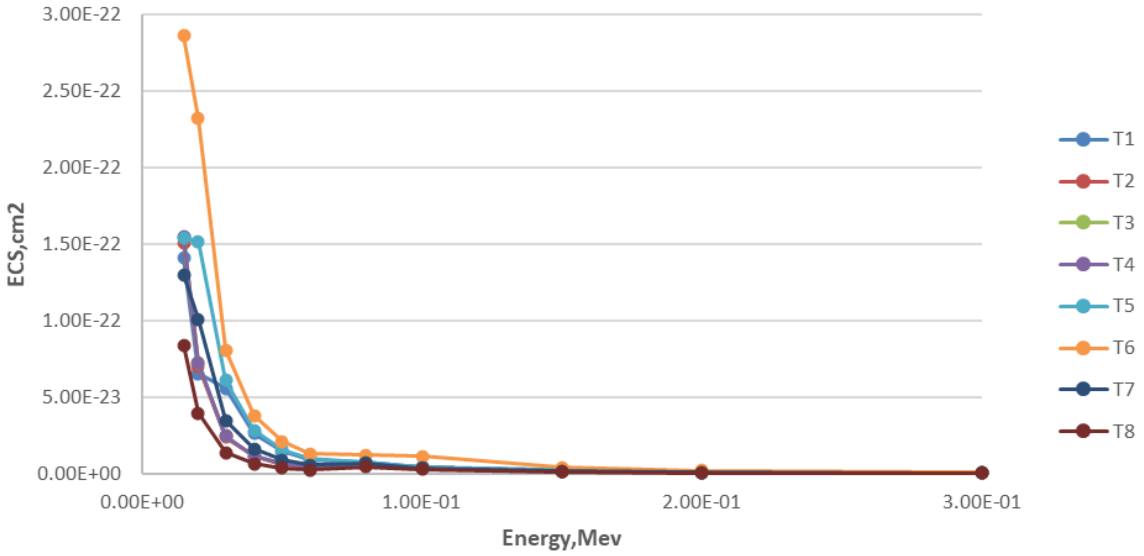

Figure (14): Gamma shielding by the tested material according to the ECS results.

4.10. Effective Atomic Number (Z_{eff})

This concept describes the effects of nuclear interactions and shielding and is highly dependent on the mean atomic number and density.

$$\mathbf{(Z_{eff} = Z - S) \ldots\ldots\ldots (9)}$$

Where: **Z =** actual atomic number, and **S** = shielding constant.

Increasing the number of electrons between the nucleus and the electron of interest (S value) minimizes Z_{eff}. The effective atomic number (Z_{eff}) may have the highest value at lower photon energies, where the photoelectric effect occurs.

The variation in Z_{eff} can be distinguished according to the tested energies, where the highest Z_{eff} values are found in the low-energy region (photoelectric absorption, the dominant process), whereas the minimum values are associated with Compton scattering. The Zeff values depend on the chemical composition of the tested material (Figure 15).

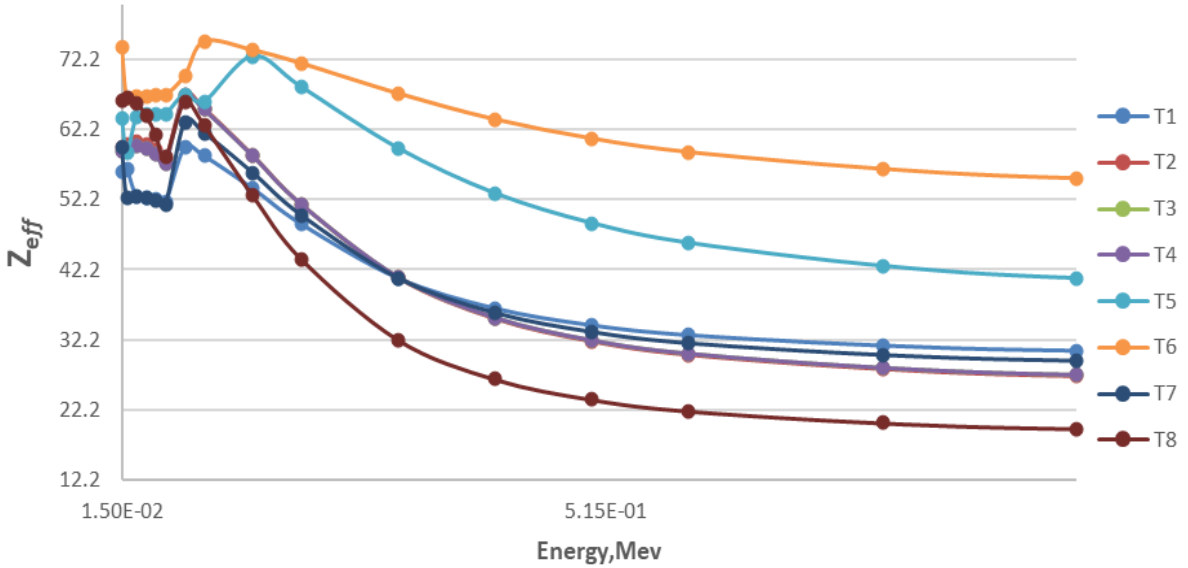

Figure (15): Gamma shielding by the tested material according to the Z_{eff} results.

5. Conclusions

The best shielding material to protect workers who deal with Gamma radiation, particularly in the research, medical, industrial, and petroleum sectors, especially Naturally Occurred Radioactive Materials (NORM) at high exposure energies, should be chosen. Various tantalum oxides were tested for gamma shielding by using a computer-based Phy-X method. Increased radiation protection depends on the density, the atomic number of a material, and the thickness.

Here, the shielding results indicate that a higher density and greater atomic number result in superior shielding properties, where the LAC and MAC decrease with increasing energy, whereas the other tested parameters increase with increasing energy. At high energies, the best material with a high atomic weight positive ion (Bi^{2+}) that can be used as a gamma ray shield is $Bi(Ta,Nb)O_4$.

Conflict of Interest: The authors declare that there are no conflicts of interest associated with this research project. We have no financial or personal relationships that could potentially bias our work or influence the interpretation of the results.

References.

[1] M. Sayyed, B. Albarzan, A. Almuqrin, A. El-Khatib, A. Kumar, D. Tishkevich, A. Trukhanov, M. Elsafi, "Experimental and Theoretical Study of Radiation Shielding Features of CaO-K_2O-Na_2O-P_2O_5 Glass Systems," *Materials*, vol. 14, article number 3772, 2021.

[2] B. Aygün, "High alloyed new stainless steel shielding material for gamma and fast neutron radiation," *Nuclear Engineering and Technology*, vol. 52, no. 3, pp. 647-653, 2020.

[3] Y. Itas, A. Alsuhaibani, A. Refat, M. Refat, A. El-Rayyes, and M. Alrahili, "Studies of Gamma Ray Shielding Properties of Lead-Free Tungsten-Borate-Tellurite Glasses (xWO_3-$20B_2O_3$-$(80-x)TeO_2$); (x = 10, 15, 20 and 25)," *Journal of Electronic Materials*, vol. 53, pp. 5696–5705, 2024.

[4] R. Ihsani, H. Heryanto, P. Gareso, and D. Tahir, "Innovative radiation shielding: a review natural polymer-based aprons with metal nanoparticle fillers," *Polymer-Plastics Technology and Materials*, vol. 63, no. pp. 738–755, 2024.

[5] F. Al-Saeedi, H. Alsafi, O. Tahlykov, M. Sayyed, H. Al Ghamdi, E. Kolobkova, F. Kapustin, A. Almuqrin, and K. Mahmoud, "Fabrication, characterization, and gamma-ray shielding performance for the lead-based Iraqi white silicate glasses: A closer examination," *Opik*, vol. 260, article number 169103, 2022.

[6] H. Gökçe, O. Güngörb, and H. Yılmaz, " An online software to simulate the shielding properties of materials for neutrons and photons: NGCal," *Radiation Physics and Chemistry*, vol. 185, article number 109519, 2021.

[7] A. Sameer and A. Ali, "Gamma-Ray Shielding Effectiveness of Clay and Boron Doped Clay Material at Different Thicknesses," *Iraqi Journal of Science*, vol. 63, no. 5, pp. 1961-1970, 2022.

[8] A. El-Sawy and E. Sarwat, "Comparative Study of Gamma- Ray Shielding Parameters for Different Epoxy Composites," *Baghdad Science Journal*, vol. 21, no. 2, pp. 0480-0495, 2024.

[9] E. Şakar, Ö.Özpolat, B. Alım, M.I. Sayyed, and M. Kurudirek," Phy-X / PSD: Development of a user friendly online software for calculation of parameters relevant to radiation shielding and dosimetry," *Radiation Physics and Chemistry***,** vol. 166, article number 108496, 2020.

[10] K. Bansal, S. Rani, N. Rani, G. Singh, and S. Singh, "Physical and Radiation Shielding Properties of Tantalum- Zinc-Sodium-Borate Glasses, " *AIP Conference Proceedings* vol. 2352, article number 050023, 2021.

[11] C. More, Z. Alsayed, M. Badawi, A. Thabet, P. Pawar, "Polymeric composite materials for radiation shielding: a review, " *Environmental Chemistry Letters*, vol. 19, pp. 2057–2090, 2021.

[12] B. Kanagaraj, N. Anand, A. Andrushia, and M. Naser, "Recent developments of radiation shielding concrete in nuclear and radioactive waste storage facilities – A state of the art review, " *Construction and Building Materials*, vol. 404, Article number 133260, 2023.

[13] B. Aygün, "Neutron and gamma radiation shielding Ni based new type super alloys development and production by Monte Carlo Simulation technique," *Radiation Physics and Chemistry*, vol. 188, article number 109630, 2021.

[14] C. Okafor, U. Okonkwo, and I. Okokpujie, "Trends in reinforced composite design for ionizing radiation shielding applications: a review, " *Journal of Materials Science*, vol. 5, pp.11631–11655, 2021.

[15] D. Shi, Y. Xia, J. Wang, F. Chen, X. Ma, Y. Zhao, M. Liu, and K. Yu, "Recycling E-waste CRT glass in sustainable geopolymer concrete for radiation shielding applications, " *Journal of Environmental Chemical Engineering*, vol. 12, Article number 114693, 2024.

[16] E. Kavaz, N. Ekinci, H. Tekin, M. Sayyed, B Aygün, and U. Perişanoğlu," Estimation of gamma radiation shielding qualification of newly developed glasses by using WinXCOM and MCNPX code, " *Progress in Nuclear Energy*, vol. 115, pp. 12-20, 2019.

[17] F. Akman, M. Kaçal, N. Almousa, M. Sayyed, and H. Polat, " Gamma-ray attenuation parameters for polymer composites reinforced with $BaTiO_3$ and $CaWO_4$ compounds, " *Progress in Nuclear Energy*, Volume 121, article number 103257, 2020.

[18] H. Bichsel and H. Schindler, The interaction of radiation with matter. In Particle Physics Reference Library Detectors for Particles and Radiation, " Vol. 2, Editors: C. Fabjan and H. Schopper, Springer, 2020.

[19] K. Filak-Mędoń, K. Fornalski, M. Bonczyk, A. Jakubowska, K. Kempny, K. Wołoszczuk, K. Filipczak, K. Żerańska, and M. Zdrojek , "Graphene-based nanocomposites as gamma- and X-ray radiation shield," *Scientific Reports* vol. 14, Article number 18998, 2024.

[20] N. AbuAlRoos, M. Azman, N. Amin, and R. Zainon, " Tungsten-based material as promising new lead-free gamma radiation shielding material in nuclear medicine, " *Physica Medica*, vol. 78, pp. 48-57, 2020.

[21] Y.Wu, Y. Cao, Y. Wu, and D. Li, "Mechanical Properties and Gamma-Ray Shielding Performance of 3D-Printed Poly-Ether-Ether-Ketone/Tungsten Composites, " *Materials (Basel, Switzerland)*,vol. 13,no. 20, pp. 4475, 2020.

[22] S. Barbhuiya, B. Das, P Norman, and T. Qureshi, "A comprehensive review of radiation shielding concrete: Properties, design, evaluation, and applications," *Structural Concrete*, vol. 2024, pp. 1–47, 2024.

[23] A. Acevedo-Del-Castillo, E. Águila-Toledo, S. Maldonado- Magnere, and H. Aguilar-Bolados, "A Brief Review on the High-Energy Electromagnetic Radiation-Shielding Materials Based on Polymer Nanocomposites, " *International Journal of Molecular Sciences*, vol. 22, no. 16, pp. 9079, 2021.

[24] H. Tekin, S. Issa, G. Kilic, H. Zakaly, M. Abuzaid, N. Tarhan, K. Alshammari, H. Sidek, K. Matori, andM. Zaid, "In-Silico Monte Carlo Simulation trials for investigation of V_2O_5 Reinforcement Effect on Ternary Zinc Borate Glasses: nuclear radiation shielding dynamics. *Materials (Basel, Switzerland)*, vol. 14, no. 5, pp. 1158. 2021.

[25] N. Salman and K. Hammud, "Phy-X/PSD and NGCAL Models of Several Metal Sulphides: Theoretical Prediction of Gamma Shielding Efficiency," *Iraqi Journal of Industrial Research*, vol. 11, no. 3, pp. 94–118, 2024.

[26] Ralph, J., Von Bargen, D., Martynov, P., Zhang, J., Que, X., Prabhu, A., Morrison, S. M., Li, W., Chen, W., & Ma, X. (2025). Mindat.org: The open access mineralogy database to accelerate data-intensive geoscience

research. American Mineralogist, 110(6), 833–844. doi:10.2138/am-2024-9486. [Online]. Available: https://www.mindat.org.

[27] J. Zaidan, "Natural Occurring Radioactive Materials (NORM) in the oil and gas industry," *Journal of Petroleum Researches and Studies*, vol. 1, no. 1, pp. 3-18, 2010.

[28] J. Popic, L. Urso, and B. Michalik, "Assessing the exposure situations with naturally occurring radioactive materials across European countries by means of the e-NORM survey," *Science of the total Environment*, vol. 905, Article Number 167065, 2023.

[29] A. Al-Rubaye, D. Jasim, H. Al-Robai, H. Al-khafaj, H. Ameen, and A. Al-Turaihi, "Risks of Naturally Occurring Radioactive Material Exposure on the Environment in Oil and Gas Field," *IOP Conference Series: Earth and Environmental Science*, vol. 1371, article number 022022, 2024.